KeAi

CHINESE ROOTS
GLOBAL IMPACT

#### Contents lists available at ScienceDirect

# Petroleum Science

journal homepage: www.keaipublishing.com/en/journals/petroleum-science



# Original Paper

# Mechanical synergistic interaction between adjacent corrosion defects and its effect on pipeline failure



Wei Wang a, b, Yi Zhang a, b, \*, Jian Shuai a, b, Yi Shuai a, b, \*\*, Lei Shi c, Zhi-Yang Lv a, b

- <sup>a</sup> College of Safety and Ocean Engineering, China University of Petroleum, Beijing, 102249, China
- <sup>b</sup> Key Laboratory of Oil and Gas Safety and Emergency Technology, Ministry of Emergency Management, Beijing, 102249, China
- <sup>c</sup> Sinopec (Dalian) Research Institute of Petroleum and Petrochemicals Co., Ltd, Dalian, Liaoning, 116014, China

#### ARTICLE INFO

# Article history: Received 23 October 2022 Received in revised form 22 February 2023 Accepted 22 February 2023 Available online 2 March 2023

Edited by Jia-Jia Fei

Keywords:
Pipelines
Adjacent defects
Interaction
Failure position
Finite element model

#### ABSTRACT

This work provides a new comprehensive assessment method to determine the complex mechanical interaction of adjacent corrosion defects. Firstly, a three-dimensional (3D) finite element model of pipelines containing adjacent defects (involving longitudinally aligned, circumferentially aligned, and diagonally aligned defects) was developed and validated by full-scale burst tests. Then, the synergistic stress interaction between adjacent defects was analyzed, and the relationship between the burst position of the pipeline and defect spacing was determined. At last, the applicability of several commonly used critical spacing rules for identifying the interaction between adjacent defects was compared and discussed in detail. The results show that the failure position of the pipeline containing adjacent defects is related to the relative position of defects. For longitudinally aligned corrosion defects, the stronger the interaction between defects (i.e., the shorter the distance between two defects), the closer the failure position of the pipeline to the center of the defect spacing. For circumferentially aligned corrosion defects, the failure position of the pipe tends to move from the defect edge to the geometric center of the defect with increasing defect spacing. For diagonally aligned defects, the failure position is generally located on the path connecting the defect and the spacing. The currently available evaluation criteria for identifying circumferentially interacting defects display the most accuracy, and the identification effect of diagonally aligned defects is the poorest. In addition, the critical spacing rule proposed by Li presents the highest precision in identifying the interacting defects. The results are expected to provide a stress synergistic failure assessment method for pipelines containing cluster corrosion defects in engineering. © 2023 The Authors. Publishing services by Elsevier B.V. on behalf of KeAi Communications Co. Ltd. This is an open access article under the CC BY-NC-ND license (http://creativecommons.org/licenses/by-nc-nd/ 4.0/).

# 1. Introduction

Due to the existence of pollutants in the medium of soil and pipes, oil and gas pipelines are extremely vulnerable to corrosion in service (Cheng, 2016; Shuai et al., 2021, 2022a, b; Ma et al., 2013; Zhu, 2021; Shuai et al., 2022a, b). Corrosion defects lead to the thinning of pipe walls. At the same time, there is a reduction in the pressure-bearing capacity of the pipeline (Chen et al., 2015; Kere and Huang, 2022; Chauhan and Swankie, 2015; Gao et al., 2019; Chen et al., 2022; Filho et al., 2014). The pipeline will form

E-mail addresses: reckonyee@163.com (Y. Zhang), yshuai@cup.edu.cn (Y. Shuai).

perforation when the wall thickness is thinned to a certain extent. This has led to frequent leakage or rupture accidents, resulting in economic losses and security risks (Cronin and Pick, 2002; Wang et al., 2022a, b; Keshtegar and Seghier, 2018).

Generally, corrosion defects on a buried oil/gas pipeline can be divided into multiple defect clusters and single defects (Benjamin and Cunha, 2007; Chiodo and Ruggieri, 2009). The failure pressure of a pipeline containing multiple defects is lower than that of a pipeline containing each of the same defects (Bao and Zhou, 2021; Wang et al., 2021; Benjamin et al., 2016a, b; Chen et al., 2015). According to current research, it is clear that the geometry, spacing, and orientation of defects are important factors affecting the failure pressure of pipelines containing multiple defects.

Experimental tests, numerical simulations and a combination of both are currently the main methods used to determine the failure pressure of pipelines containing multiple defects. In the

<sup>\*</sup> Corresponding author. College of Safety and Ocean Engineering, China University of Petroleum, Beijing, 102249, China

<sup>\*\*</sup> Corresponding author. College of Safety and Ocean Engineering, China University of Petroleum, Beijing, 102249, China

#### Nomenclature

D Diameter of pipeline d Depth of adjacent defects  $d_1, d_2$ Depth of defect 1 and defect 2 Е Young's modulus L Length of adjacent defects  $L_1$ ,  $L_2$ Length of defect 1 and defect 2  $S_L$ Longitudinal spacing Longitudinal limit spacing  $S_C$  $S_{\tau}^{\widetilde{L}im}$ Circumferential spacing  $S_C^{Lim}$ Circumferential limit spacing t Thickness of pipeline wall Width of adjacent defects w Poisson's ratio Yield stress  $\sigma_{\nu}$ Ultimate tensile stress  $\sigma_u$ 

experimental method, the failure pressure of a pipeline containing multiple defects is assessed by preparing different types of defects on the surface of the pipe and by conducting a full-scale test. At first, the failure pressure of a pipeline containing a single defect is evaluated. Then, the failure pressure of a pipe containing multiple defects is obtained by testing. Finally, the ratio of the failure pressure of a pipeline containing multiple defects to that of a single defect is used to identify the interacting defects. A series of burst tests have been carried out on different steel grades (Benjamin et al., 2007, 2016; Freire et al., 2011a, b). Benjamin et al. (2005) conducted full-scale experiments with double and quadruple interacting defects in the presence of interactions and compared them with the failure pressure of a pipeline predicted by present standards. Based on the outcomes of the external interacting defects, Idris et al. (2021) investigated the rule of radial interacting defects by carrying out full-scale burst tests. However, the experimental method is costly, and it is difficult to determine the failure pressure of a pipeline containing interacting defects in a timely manner. Numerical simulations have been developed as an alternative to predict the failure pressure of pipelines containing interacting defects. In the numerical simulation method, the finite element model developed by solid elements has been used to investigate the failure behaviour of pipelines containing interacting defects (Cosham and Hopkins, 2004; Liu et al., 2009; Al-Owaisi et al., 2018). Soares et al. (2019) simulated the coupled thermomechanical phenomenon of pipelines containing interacting defects under internal pressure and thermal loading. They found that thermal loading significantly reduces the failure pressure of corroded pipelines containing interacting defects. Velázquez et al. (2022) established a finite element model to investigate the influence on the mechanical behaviour of ageing pipelines with local and global corrosion. They found that taking into account the effect of the ageing material of the pipeline, the failure pressure of the corroded pipeline could be predicted more accurately. Zhou et al. (2022) constructed a finite element model of a high-grade steel pipeline containing group corrosion and discussed the failure mechanism of a pipeline containing multiple defects. The results showed that the deepest defect is the primary factor for determining the failure pressure of a pipeline containing multiple defects.

The DNV RP-F101 provides a convenient method for predicting the failure pressure of pipelines containing multiple defects. In this method, the failure pressure of a pipeline containing multiple defects is equivalent to the minimum failure pressure of a pipeline containing any combination of double defects (Fu and Batte, 1999; McNealy et al., 2008; ASME, 2012). To determine the failure pressure of a pipeline containing double defects, it is necessary to identify whether there is an interaction between the adjacent defects. The interaction of defects is determined by the defect spacing. If the defect spacing is less than the limit spacing in any direction, the interaction of the defects is taken into account. The geometry of interacting defects and the defect spacing are equivalent to the geometry of a single defect (McNealy et al., 2008). In other words, the failure pressure of a pipeline containing double defects is the failure pressure of the pipeline containing a single defect. In contrast, there is no interaction between defects when the defect spacing is more than the critical distance. At the same time, the failure pressure of a pipeline containing double defects is equal to the minimum of the failure pressure of a pipeline containing each of the same defects. Therefore, the limit spacing of defects is crucial to predict the failure pressure of a pipeline containing multiple defects.

The rule for interaction between defects is to determine the limit spacing for interaction between defects in the longitudinal and circumferential directions. Table 1 shows the limit spacing for interaction between adjacent defects according to the research results of longitudinally and circumferentially aligned defects. As shown in Table 1, numerous scholars have conducted intensive studies on the interaction rules, but there are limited investigations focusing on the mechanical interaction between defects on the failure behavior of pipelines. In addition, the study of the interaction between adjacent defects generally considers identical defects in the longitudinal arrangement and circumferential arrangement. which idealizes the distribution of double defects. In practice, the multiple defects are randomly arranged on a pipeline, and their geometries are different. Therefore, for defects with random distributions and nonidentical geometries, the interaction between defects still has to be further studied. This work characterizes randomly distributed defects by diagonally aligned defects and analyzes the mechanical interactions of defects with nonidentical geometries.

Considering the insufficiency of current studies, this work investigated the mechanical interaction between adjacent defects using numerical analysis methods. Finite element models of a pipeline containing adjacent defects with longitudinally, circumferentially and diagonally aligned defects were developed to analyze the failure behaviour of pipelines. The innovation of this work involved systematically investigating the influence of the mechanical interaction between defects on the failure position of pipelines. Considering random defects with nonidentical geometries, the relationship between the failure position and defect spacing under different arrangements of defects is clarified.

# 2. Numerical model

# 2.1. Aligned types of adjacent corrosion on a pipeline

According to the relative position of adjacent defects outside a pipeline, they are generally divided into longitudinal, circumferential and diagonal arrangements. To determine the arrangement of defects, it is necessary to establish the horizontal and vertical axes along the axial and circumferential directions of the pipeline and take the center of the defect as the origin. If the horizontal axis between the defects is completely overlapped, the defects are longitudinally aligned defects. If the vertical axis between defects is completely overlapped, the defects are circumferentially aligned defects. When the horizontal and vertical axes of the defects do not overlap, the defects are diagonally aligned.  $S_L$  is the longitudinal spacing between defects and  $S_C$  is the circumferential spacing

 Table 1

 Interaction rules between adjacent defects according to the literature.

Reference	Longitudinal limit spacing, $S_L^{\it lim}$	Circumferential limit spacing, $S_C^{\it Lim}$			
CW (Coulsen and Worthingham, 1990)	$S_L^{lim} = \min(L_1, L_2)$	$S_C^{lim} = \min(w_1, w_2)$			
Pipeline operator forum (Pitchford, 1999)	$S_L^{Lim} = \min(6t, L_1, L_2)$	$S_C^{Lim} = \min(6t, w_1, w_2)$			
DNV RP-F101 (2010)	$S_I^{Lim} = 2.0\sqrt{Dt}$	$S_C^{Lim} = \pi \sqrt{Dt}$			
API 579 (2007)	$S_L^{Lim} = (L_1 + L_2)/2$	$S_C^{Lim} = (w_1 + w_2)/2$			
ASME B31G (2012)	$S_L^{Lim} = 3t$	$S_C^{Lim} = 3t$			
BS 7910 (2013)	$S_I^{Lim} = 2.0\sqrt{Dt}$	$S_C^{Lim} = 3.0\sqrt{Dt}$			
Silva et al. (2007)	$S_I^{Lim} = 2.0\sqrt{Dt}$	$S_C^{Lim} = 2.0\sqrt{Dt}$			
Al-Owaisi et al. (2016)	$S_I^{Lim} = 3t$	$S_C^{Lim} = t$			
Li et al. (2016)	$S_L^{Lim} = 2.0\sqrt{Dt}(L \le \sqrt{20Dt})$	$S_C^{Lim} = 0.1\pi D(L \le \sqrt{20Dt})$			
	$S_L^{Lim} = 1.0\sqrt{Dt}(\sqrt{20Dt} \le L \le \sqrt{50Dt})$	$S_C^{Lim} = 0.05\pi D(\sqrt{20Dt} \le L \le \sqrt{50Dt})$			
	$S_L^{Lim} = t(L > \sqrt{50Dt})$	$S_C^{Lim} = t(L > \sqrt{50Dt})$			
Sun and Cheng (2018)	$S_L^{Lim} = 2.5\sqrt{Dt}$	$S_C^{Lim} = 5.3t$			

between defects. The distribution of adjacent defects is determined by  $S_L$  and  $S_C$ . The distribution of different adjacent defects is shown in Fig. 1.

#### 2.2. Properties of material

To simulate the elastic-plastic behaviour of the pipeline under internal pressure, the material properties need to be set in the pretreatment process. The finite element model of pipelines is established by a pipeline with a diameter of 357 mm, and a wall thickness of 10 mm. The specific dimension and material properties of the pipeline are shown in Table 2.

#### 2.3. General

Finite element models of corroded pipelines containing longitudinally, circumferentially and diagonally aligned defects are developed by using the finite element method. It has been reported by Fatemi and Kenny (2011) that the FE modelling results are in good agreement with the experimental results when the modeled length of the pipeline exceeds 3.5 times of diameter *D*. Therefore,

**Table 2**The dimension and material properties of the pipeline.

Steel	D, mm	t, mm	E, MPa	ν	$\sigma_y$ , MPa	$\sigma_u$ , MPa
X52	357	10	$2.1\times10^{5}$	0.3	358	455

the length of the pipe model used in the FE analysis was set to be 2000 mm to avoid the end effect on the stress state of defect area. To simulate the geometry of defects on the pipeline, a twenty-node SOLID186 element type was selected to discretize the pipe for its good performance in solving the nonlinear problems of plasticity, large displacements, and strains. In the modelling process, the corrosion defect is assumed as a rectangular shape, where the corners of the rectangular defect are chamfers as an arc-transition to avoid stress concentration. The element is able to solve the nonlinear problems of plasticity, large displacements and strains. Chamfering is the cutting of a sphere of the same radius as the depth of the defect in a square of equal wall thickness. In other words, the depth of the chamfer is equal to the depth of the defect.

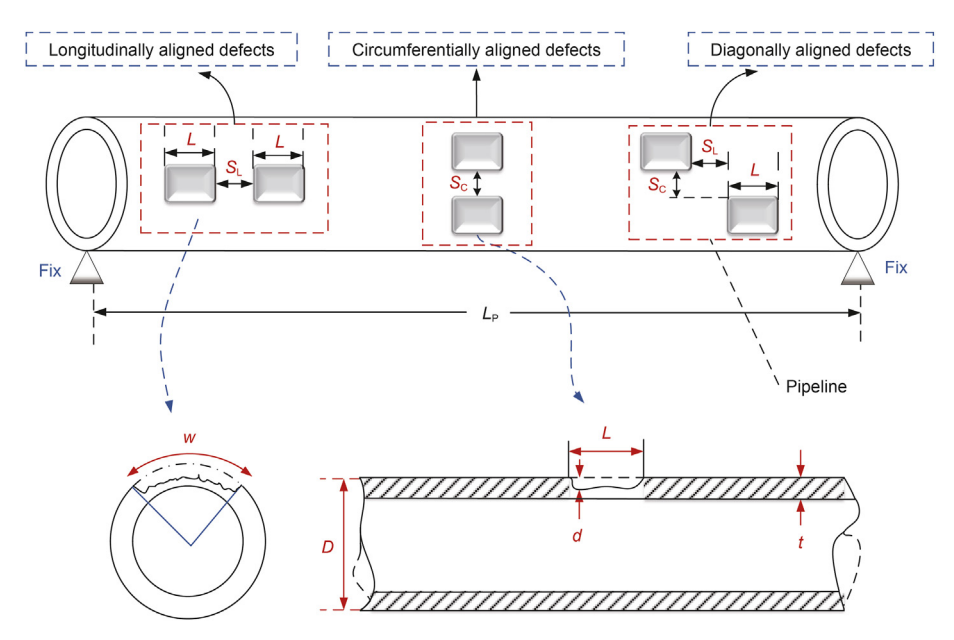


Fig. 1. The various orientation of adjacent defects.

#### 2.4. Study of mesh density convergence

The FE model containing double defects is constructed by three-dimensional solid elements, so the mesh density in the axial, circumferential and radial directions of the pipe will affect the mechanical interaction between defects. This section first analyzes the mesh convergence in the circumferential and axial directions. The mesh dimensions are represented by  $m_c \times m_l$ , where  $m_c$  represents the mesh size along the circumferential direction of the pipe, and  $m_l$  is the mesh size along the axial direction of the pipe. Considering the high stress gradient in the defect and spacing regions, the grids in this local area should be encrypted. Fig. 2 displays the effect of grid density of the FE model on the burst pressure of the pipeline containing double defects with a length of 200 mm and a depth of 5 mm.

As shown in Fig. 2(a), the burst pressure decreases as the number of grids in the defect region continues increase. The failure pressure of the pipeline tends to be stable when the mesh size of the defect area reaches  $2\times 6$ . This indicates that the mesh size satisfies the convergence condition. For the intact region, it can be seen from Fig. 2(b) that when the mesh density attains  $30\times 33$ , the failure pressure changes slightly compared to the grid size of  $40\times 33$ , which achieves the convergence criteria for meshing.

In the wall thickness direction, the influence of meshes with 1–6 layers on the failure pressure of the pipe is discussed, as shown in Fig. 3. For longitudinally aligned defects, the failure pressure of the pipeline remains stable when the number of mesh layers comes to 2. For circumferentially aligned defects, the burst pressure tends to be uniform for more than 3 layers of the mesh. It has a negligible error of 2.38% compared to the failure pressure under a two-layer grid.

On the basis of the above analysis of the influence of mesh density on the failure pressure of the pipeline, the mesh size for the defect area is determined as  $2 \text{ mm} \times 5 \text{ mm}$  and the mesh size of the nondefect area is  $33 \text{ mm} \times 30 \text{ mm}$ . Two layers of the grid were divided along the wall thickness direction, and the specific mesh dimensions are shown in Fig. 4.

Upon observation, it can be noted from Fig. 4(b)–(c) that the area where the defect spacing joins the defect below appears a mesh discontinuity. The grid disconnection in Fig. 4(b) is induced by the inconsistent geometries of the two defects. The mesh separation of the defect spacing and defects in Fig. 4(c) occurs because of the randomness of the relative positions of the diagonally aligned defects. At the same time, an overlapping area exists between the two defects in the axial or circumferential projection when  $S_I < 0$  or  $S_C < 0$ .

To address this issue, the Multi-Point Coupling (MPC) method was adopted to connect the mesh separations. An FE model

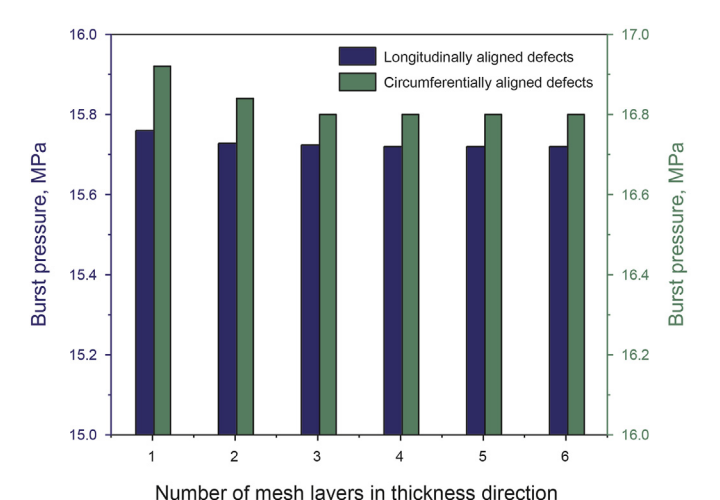
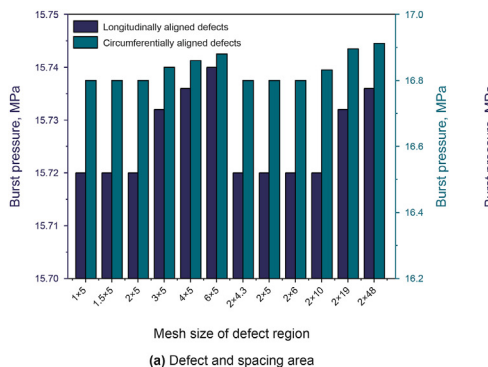


Fig. 3. Mesh layers along the ligament of the FE model.

containing circumferentially aligned defects with a depth of 3 mm and lengths of 126 mm and 96 mm respectively was performed to verify the feasibility of the MPC method. Mesh alignment of this model can be achieved by setting the mesh length of the defect area to 5 mm. Node merging and MPC methods were subsequently applied to connect the defect spacing and the defect. The failure pressure when the burst occurred was 23.08 MPa for both methods, indicating that the two methods have no distinction in the failure behaviour of pipes containing corrosion defects. In contrast, the node merging method restricts the choice of defect geometry, so the MPC method was substituted for model construction.

### 2.5. Loads and boundary conditions

The finite element model was constructed according to the orientation of the adjacent defects. For longitudinally and circumferentially aligned defects, the model was simplified to a 1/4 model or 1/2 model according to whether the geometrical characteristics of the defects are identical. For symmetrical defects, there are two circumferential symmetry planes and a longitudinal symmetry plane in the quarter model. For the model with asymmetrical defects, there are two circumferential symmetry planes in the longitudinally aligned defects. The circumferentially aligned defects have an axial symmetry plane, which is the circumferential section of the axial center of defects. However, there is an overlap in longitudinal or circumferential projections for diagonally aligned defects. It is necessary to establish a complete model of a corroded



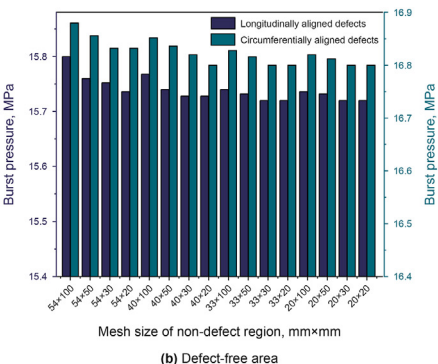
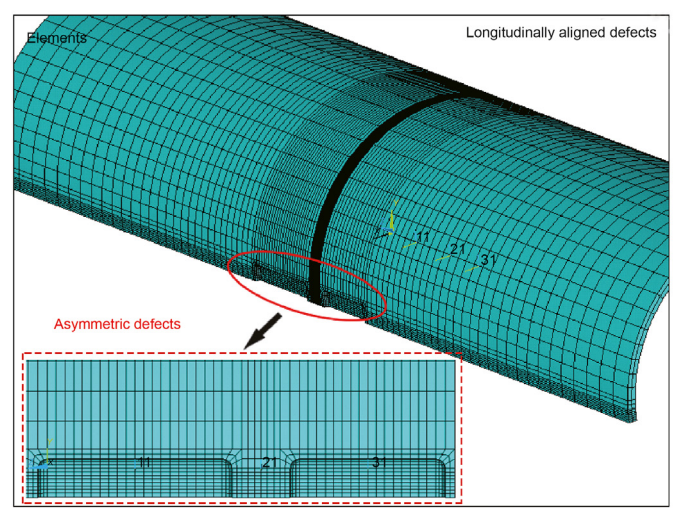
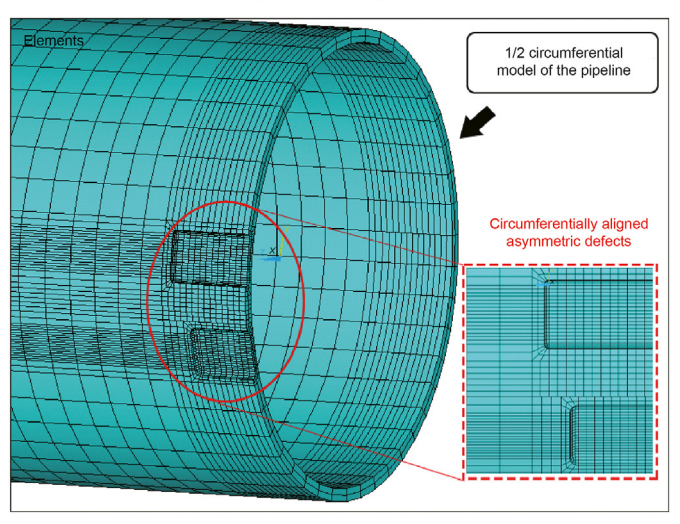


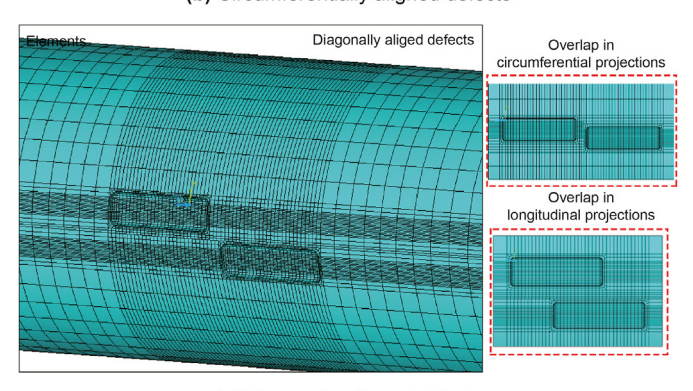
Fig. 2. Effect of the mesh density of the FE model on the failure pressure.



(a) Longitudinally aligned defects



(b) Circumferentially aligned defects



(c) Diagonally aligned defects

Fig. 4. The grid of the finite model of a pipeline containing adjacent defects.

pipeline. The load of the pipeline is only considered internal pressure. Symmetrical constraints were applied to the symmetrical plane of the simplified model. The displacements of the uncorroded end of the pipeline in the Y direction and the Z direction are constrained in the polar coordinate system.

#### 2.6. Failure criterion

To investigate the effect of interactions between adjacent defects on the stress state of the defect region at the moment of pipeline failure, it is necessary to determine the critical stress state for the failure of the pipe. At present, the ultimate tensile strength stress criterion (Zhu, 2021: Shuai et al., 2022a, b: Bao and Zhou, 2021; Zhang and Zhou, 2020, 2021, 2022; Cabral et al., 2022) is widely used to determine the burst pressure of pipelines containing defects. Shuai et al. (2022a, b) predicted the failure pressure of a pipeline containing a single defect under the combined loads of axial compression force and bending moment based on this criterion. Bao and Zhou (2021) applied this criterion to evaluate the burst pressure of a finite element model of a pipe containing defects. This criterion indicates that burst failure occurs when the Mises equivalent stress on the thickness of the ligament in the defect region reaches the ultimate tensile strength of the material. Therefore, this criterion is applied to determine the stress state of the pipeline when burst failure occurs.

### 2.7. Verification of the numerical model with experimental data

In order to verify the reliability of the finite element model of adjacent defects in practice, the results of FE analysis in this work were verified by the results of burst tests in Benjamin and Freire's work (Benjamin et al., 2005). The steel grade of the tested pipeline was X80. The diameter and wall thickness of the pipeline were 458.8 mm and 8.1 mm, respectively. The parameters of the defects in the experiments and the results of burst tests and the finite element method are shown in Table 3.

As can be seen in Table 3, the average error between the failure pressure of a pipeline containing adjacent defects predicted by the finite element method and the burst test results is 2.53%. The simulation result for diagonally aligned defects has a larger error of 4.57% than the test results. This indicates that the simulation results are in good agreement with the corresponding experiments, which demonstrates that the finite element model developed in this work has acceptable accuracy for predicting the failure pressure of pipelines containing adjacent defects.

# 3. Results and discussion

# 3.1. Longitudinally aligned symmetrical defects

The longitudinally aligned symmetrical defects mean that the horizontal line of adjacent defects is located on the same axis, and the geometries of defects are identical. The influences of the length, depth and spacing of defects on the failure process of a pipeline containing longitudinally symmetrical defects were analyzed. The width of defects is uniform to 40 mm because the width of a defect has little effect on the failure pressure of pipelines containing volumetric defects (Ma et al., 2013; Cabral et al., 2022). The specific parameters of cases containing longitudinally symmetrical defects are summarized in Table 4.

Taking longitudinally symmetrical defects with a length of 200 mm and a depth of 5 mm as an example, the distribution of the von Mises stress when the pipeline fails is shown in Fig. 5. It can be seen that the equivalent stress at the defect center gradually increases and the equivalent stress in the spacing between defects gradually decreases with the increase of longitudinal spacing.

Fig. 6 depicts the variation in the failure position with longitudinal spacing for pipes containing longitudinally symmetrically

 Table 3

 Verification of the finite element model of adjacent defects.

Specimen	Orientation	d, mm	L, mm	w, mm	$S_L$ , mm	$S_C$ , mm	P <sub>EXP</sub> , MPa	$P_{FEM}$ , MPa	Error, %
IDTS2	Single	5.39	39.6	31.9	_	_	22.679	22.58	0.44
IDTS3	Longitudinal	5.32	39.6	31.9	20.5	_	20.314	20.63	1.56
IDTS4	Circumferential	5.62	39.6	32.0	_	9.9	21.138	21.44	1.43
IDTS5	Diagonal	5.42	39.5	32.1	-9.5	10.0	20.873	19.92	4.57
Mean	_	_	_	_	_	_	_	_	2.00

Note: Error (%)=(ABS  $(P_{EXP}-P_{FEM})/P_{EXP}) \times 100$ .

**Table 4**Geometries and spacing of longitudinally symmetrical defects.

L, mm	d, mm	$S_L$ , mm	$L/\sqrt{Dt}$	d/t	$S_L/\sqrt{Dt}$
60, 120, 200, 267, 350, 400, 500, 800,	3, 5, 7	18, 30, 60, 90, 120, 180	1, 2, 3.35, 4.47, 5.85, 6.69, 8.36, 13.39	0.3, 0.5, 0.7	0.3, 0.5, 1, 1.5, 2, 3

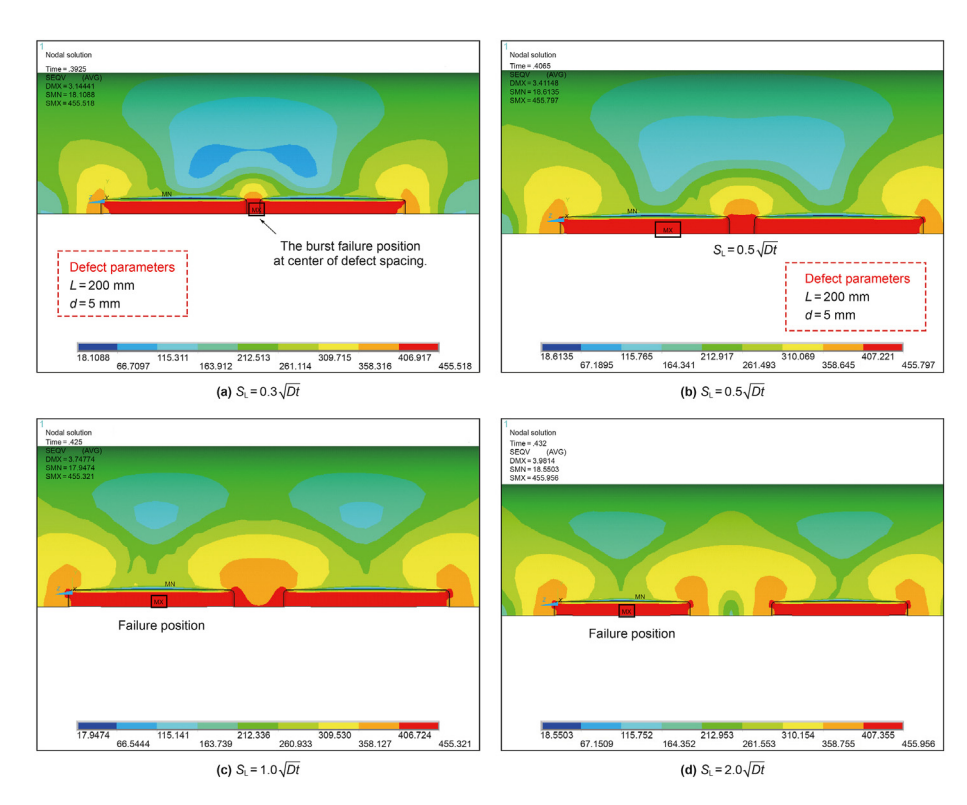


Fig. 5. The von Mises stress distribution of a pipeline containing longitudinally aligned symmetrical defects.

aligned defects, where the ordinate represents the distance from the failure position to the defect center. With increasing longitudinal spacing, the location of the maximum von Mises stress transfers from the center of defect spacing to the defect center. The burst failure position, i.e., the maximum von Mises stress, is observed to occur at the defect spacing center when  $S_L = 0.3 \sqrt{Dt}$ . As the defect spacing  $S_L$  increases to  $S_L = 0.5 \sqrt{Dt}$  and  $S_L = 1.0 \sqrt{Dt}$ , the von Mises stress at the center of the corrosion defect increases gradually, and the position of the maximum von Mises stress also moves towards the defect center. On the contrary, the von Mises stress around the spacing of the defect decreases. For a pipe with longitudinally aligned symmetrical defects with  $S_L = 2.0 \sqrt{Dt}$ , the failure position of the pipeline is consistent with that of a pipeline containing a single defect with identical geometry.

To intuitively describe the variation in the interaction between defects with longitudinal spacing, Fig. 7 shows the von Mises stress

changes of the center node of the defect and spacing. It can be seen from the Fig. 7 that the von Mises stress at the defect center rises continuously with increase of the  $S_L$ . When the  $S_L$  increases to 2.0  $\sqrt{Dt}$ , the error in the equivalent stress at the center of the defect compared to the center of the single defect is 0.48 MPa. This indicates that the stress interaction between defects can be neglected at  $S_L = 2.0 \sqrt{Dt}$ .

To explain the mechanism of the variation in the failure location with the defect spacing for longitudinally aligned defects, Figs. 8 and 9 illustrate the stress variation at the center node of the defect and spacing. Hoop and axial stress constitute the main stress states at the critical nodes. As can be seen in Figs. 8(a) and 9(a), the hoop and axial stress at the center of the defect gradually increase with the increase in the  $S_L$  due to the increased bulging of the defect area. For the stress state in the center of the spacing in Figs. 8 and 9(b), the stress tends to decrease with the increase in spacing. The

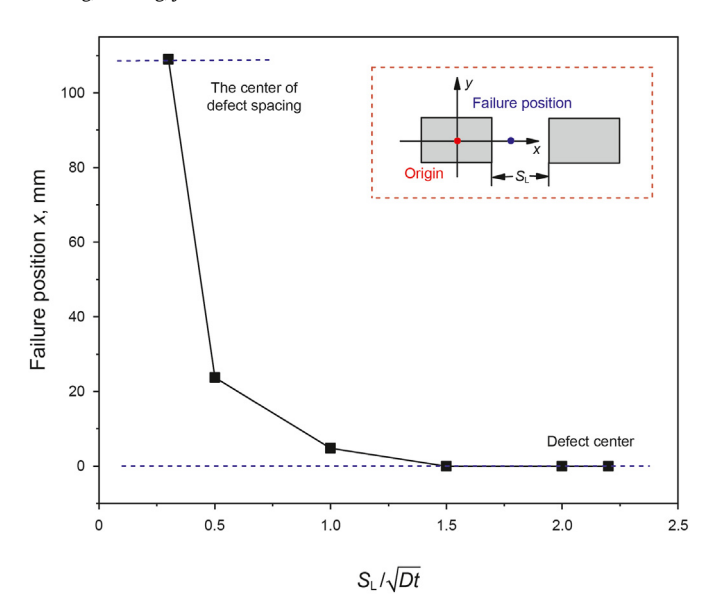


Fig. 6. Variation in the failure position with axial spacing for longitudinally aligned symmetrical defects.

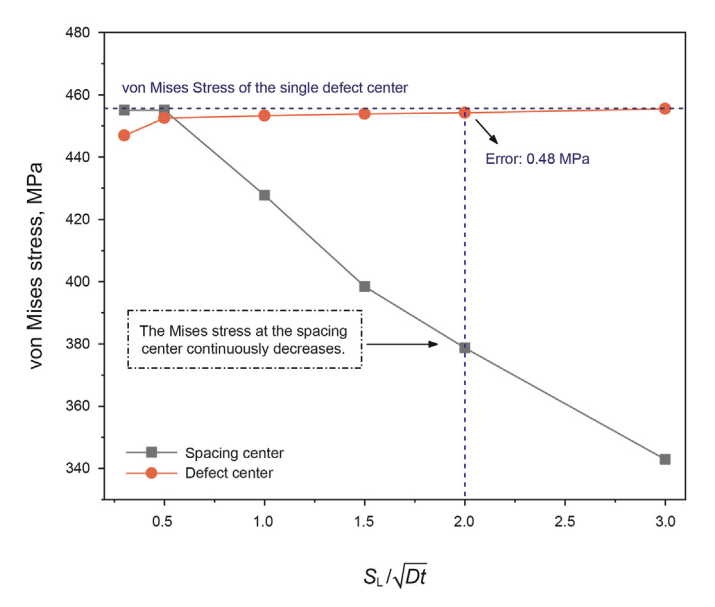


Fig. 7. von Mises stress at the center of the defect and spacing node.

above phenomenon leads to an increase in the von Mises stress at the defect center and a continuous weakening of the stress at the spacing center.

### 3.2. Longitudinally aligned asymmetrical defects

Similarly, the horizontal lines of longitudinally aligned asymmetrical defects lie on the same axis, but there are differences in the defect dimensions. The parameters of the pipeline containing longitudinally aligned asymmetrical defects include the length and depth of each defect and the longitudinal spacing between defects. The geometries and spacing of defects are listed in Table 5.

Taking longitudinally asymmetrical defects with lengths of 200 mm and 150 mm and depths of 5 mm as an example, the distribution of the von Mises stress of the pipeline is shown in Fig. 10. In this work, the more severe corrosion of the two aligned defects is defined as the base defect. Thus, the defect with a length of 200 mm is the base defect in this case. It can be seen from Fig. 10(a) that the location of the maximum von Mises stress appears in the defect spacing and is close to the base defect when  $S_I = 0.3 \sqrt{Dt}$ . As the  $S_I$  increases, the burst failure position moves to the base defect side, and the maximum von Mises stress locates in the center of the base defect when  $S_L \ge 1.0 \sqrt{Dt}$ . This is because the distributions of von Mises stress near the defect interact with each other when the spacing between the two defects is close, and the equivalent stress of the corrosion surface at the defect spacing reaches the yield state. As the defect spacing increases, the stress at the defect is symmetrically distributed on both sides of the defect center. At the same time, the von Mises stress gradually decreases in the area of defect spacing.

Fig. 11 intuitively shows the movement trend of the failure position of the longitudinally asymmetric defects with the increase of the  $S_L$ . It can be found that the failure position shifts rapidly towards the center of the defect when  $S_L \leq 1.0 \ \sqrt{Dt}$ . As the  $S_L$  increases to 1.5  $\sqrt{Dt}$ , the position at which burst failure occurs remains invariant and locates at the center of the defect. That is, when the  $S_L$  exceeds 1.5  $\sqrt{Dt}$ , the influence of the interaction on the stress field can be neglected.

# 3.3. Circumferentially aligned symmetrical defects

The circumferentially symmetrical defects are the vertical axis of the defect located in the same circumferential section, and the defect geometries are the same. The parameters of circumferentially aligned symmetrical defects include the length, depth

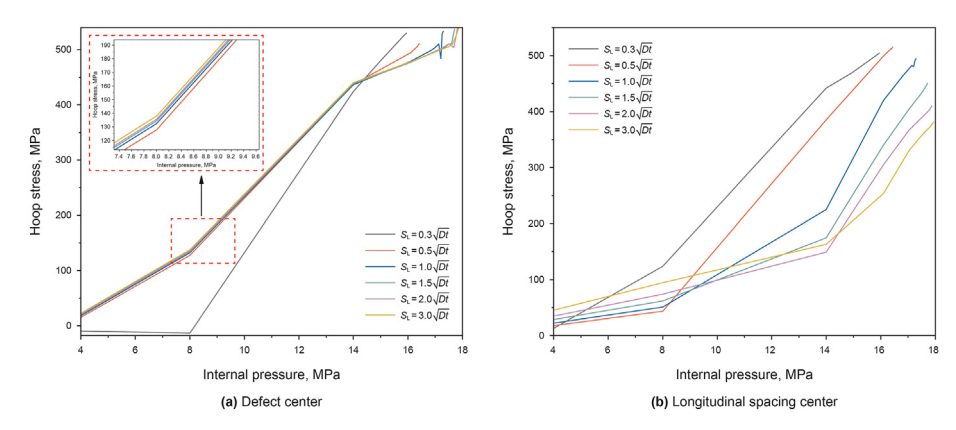


Fig. 8. The hoop stress at the center of the defect and spacing node for longitudinally aligned defects.

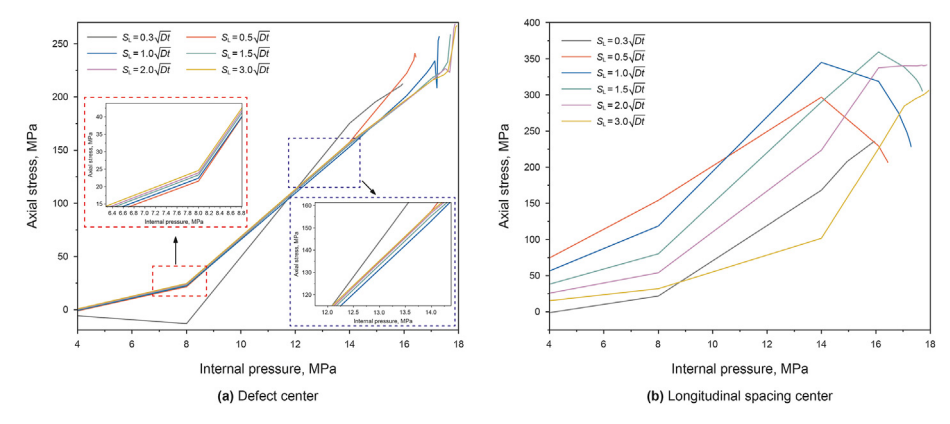


Fig. 9. The axial stress at the center of the defect and spacing node for longitudinally aligned defects.

 Table 5

 Geometries and spacing of longitudinally aligned asymmetrical defects.

$L_1/\sqrt{Dt}$	$L_2/\sqrt{Dt}$	$d_1/t$	$d_2/t$	$S_L/\sqrt{Dt}$
3.35	0.84, 1.67, 2.51	0.3, 0.5, 0.7	0.3, 0.4, 0.5, 0.6	0.3, 0.5, 1,
4.47	1.67, 3.35			1.5, 2, 3
5.85	1.67, 3.35, 5.02			
6.69	1.67, 3.35, 5.02			
8.36	1.67, 3.35, 5.02, 6.69			

spacing area gradually decreases, and it gradually increases in the geometric center of the defect. In addition, as the  $S_C$  increases, the burst failure position first moves from a location far away from the spacing to a location close to the spacing and then shifts slowly to the defect center.

In Fig. 12(a), for circumferentially symmetrical defects with  $S_C = 0.02\pi D$ , the pipeline failure occurs on the side of the defect surface away from the defect spacing. It can be observed from

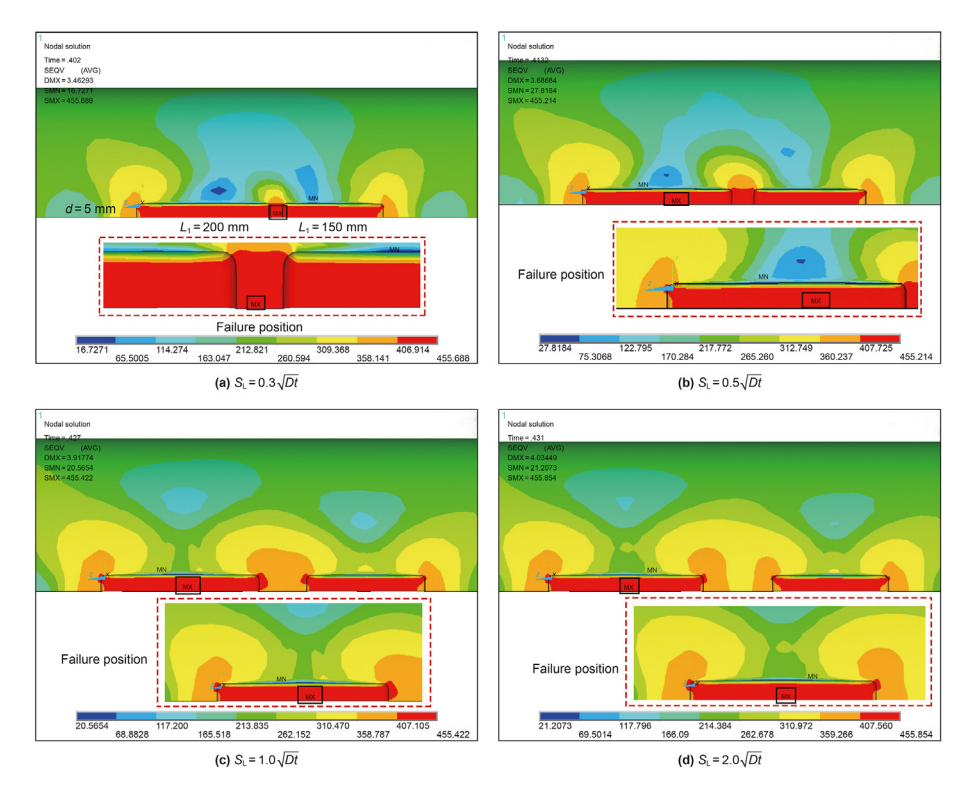
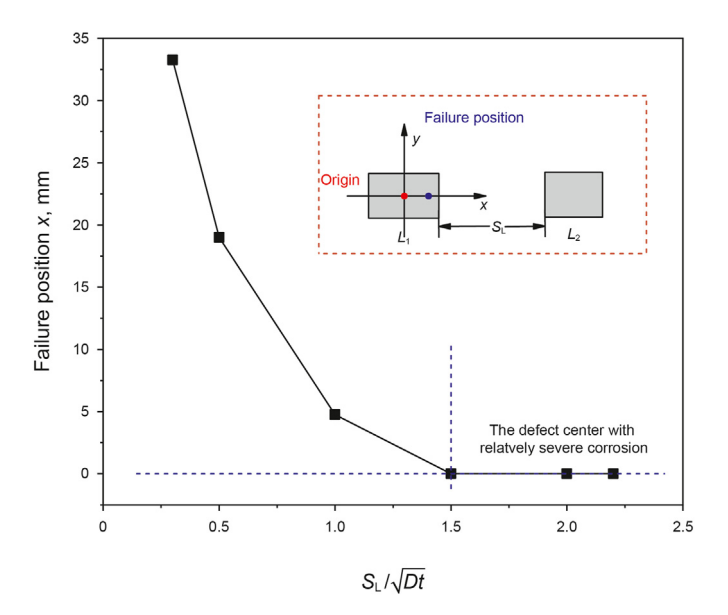


Fig. 10. The von Mises stress distribution of a pipeline containing longitudinally aligned asymmetrical defects.

and spacing of defects, where defect spacing is the circumferential spacing. Table 6 shows the specific parameters for circumferentially aligned symmetrical defects.

The distribution of von Mises stress of a pipeline containing circumferentially aligned symmetrical defects with a length of  $L/\sqrt{Dt}=3$  and a depth of d/t=0.5 is shown in Fig. 12. As the defect spacing increases, the von Mises stress in the circumferential

Fig. 12 (b) that a low von Mises stress appears in the spacing area when  $S_C=0.05\pi D$ . At the same time, the failure position transfers to the defect surface near the spacing side. As the  $S_C$  increases to  $0.1\pi D$ , the area of the low stress zone starts to expand. The low stress area in Fig. 12 (d) diffuses to the axial center of the defect when  $S_C=0.2\pi D$ . The failure position moves towards the center of one side defect. Meanwhile, the interaction of the equivalent stress



**Fig. 11.** Variation in the failure position with longitudinal spacing for longitudinally aligned asymmetrical defects.

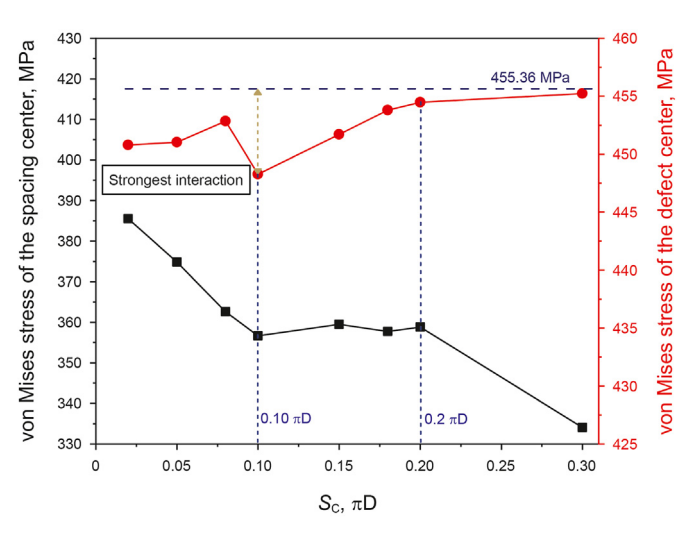


**Fig. 13.** von Mises stress at the center of the defect and spacing node for circumferentially aligned defects.

interaction can be ignored.

**Table 6**Geometries and spacing of circumferentially aligned symmetrical defects.

L, mm	d, S <sub>C</sub> , mm mm	L  √Dt d t	$S_C/\pi D$
60, 120,179, 239, 299, 358, 418, 478, 538	3, 5, 7 22.4, 33.6, 56.1, 112.1, 168.2, 201.8, 2 336.3	24.2, 1, 2, 3, 4, 5, 6, 7, 8, 9 0.3, 0.5, 0.7	0.02, 0.03, 0.05, 0.10, 0.15, 0.18, 0.20, 0.30

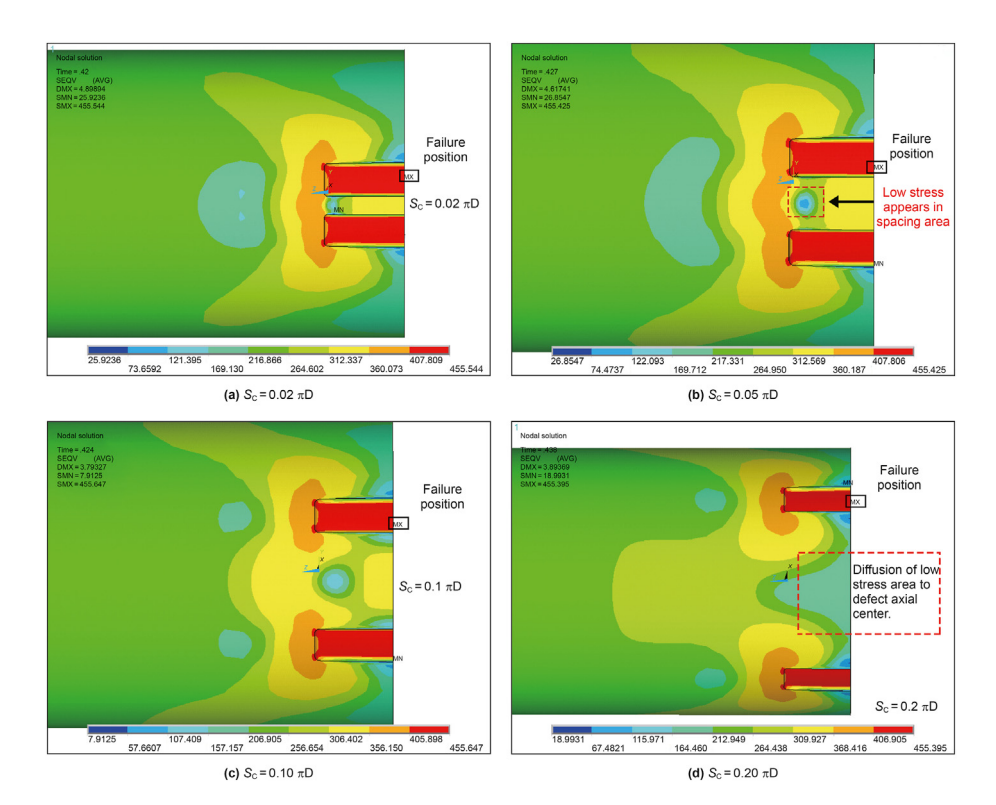


Fig. 12. The von Mises stress distribution of a pipeline containing circumferentially aligned symmetrical defects with different circumferential spacing.

field in the defect area is weak, so it can be considered that the defects are independent of each other and the circumferential Fig. 13 describes the variations in the von Mises stress at the center of the defect and the spacing with the increase in  $S_C$ . The von

Mises stress of defect center is 455.36 MPa when the pipeline containing a single defect fails. When the  $S_C$  reaches  $0.10\pi D$ , the difference in the von Mises stress of the defect center is the largest. This indicates that the interaction between defects has the most severe influence on the stress field at  $S_C = 0.10\pi D$ . In addition, the stress tolerance equals 0.21% when  $S_C = 0.20\pi D$ , suggesting that the stress interaction between defects is negligible at the spacing.

The hoop stress and axial stress curves of the defect center and spacing center are drawn in Figs. 14 and 15. The two defects and the defect spacing can be considered as a single defect when the  $S_C$  is small. The defect area suffers from internal pressure and bulges outwards. It can be seen from Figs. 14 and 15(b) that the hoop stress and axial stress in the spacing center becomes higher because the bulge center locates in the spacing area. However, the stress concentration resulting from the thinning of the wall thickness in the defect area causes higher stress at the circumferential boundary close to the defect spacing and failure occurs at this location. With the increase of  $S_C$ , the defects separate from each other, and the spacing area is no longer affected by bulging. At the same time, the hoop stress and axial stress of the defect center increase, and the failure position moves to the defect center.

# 3.4. Circumferentially aligned asymmetrical defects

There is a difference in defect geometry between circumferentially asymmetrical defects. The influencing parameters of circumferentially asymmetrical defects include the length, depth and circumferential spacing of each defect. The geometries and spacing of defects for circumferentially asymmetrical defects are shown in Table 7.

Taking the circumferentially asymmetrical defects with defect lengths of  $L_1/\sqrt{Dt}=2.1$  and  $L_2/\sqrt{Dt}=1.6$ , and defect depths of  $d_1/t=0.5$  and  $d_2/t=0.7$  as an example, the distribution of the von Mises stress for a pipeline is shown in Fig. 16. In general, defects with larger and deeper areas show more severe corrosion. The depth of the defect has more importance in affecting the failure behaviour of the pipe than a length of the defect. Therefore, the defect with a depth of d=0.7t is a severe defect in this case. For circumferentially aligned asymmetrical defects, the location of the maximum von Mises stress (i.e., failure position) of a pipeline appears on the surface of a severely corroded pipeline. That is to say, the failure pressure of a pipeline is controlled by the severe defect.

With the increases in defect spacing, the von Mises stress in the region of defect spacing gradually decreases, while the stress at the defect surface gradually increases. There is a low stress area in the defect spacing when the defect spacing increases to  $S_C=0.18\pi D$ . The distribution of the von Mises stress of the defect is symmetrical

about the circumferential center of each defect in the circumferential direction. The defects are independent of each other, and the interaction between defects is significantly weakened. In general, the interaction between defects is negligible when the defect spacing is sufficiently far. At this moment, the burst failure pressure of a pipeline containing circumferentially asymmetrical defects corresponds to the failure pressure of a pipeline containing only more severe defects.

# 3.5. Diagonally aligned defects

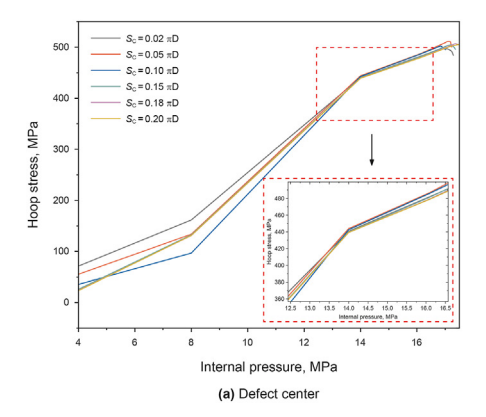
The defect spacing of diagonally aligned defects includes longitudinal and circumferential spacing. According to whether the defect spacing is greater than zero, the defects in diagonal alignment can be divided into three arrangements: an overlap of longitudinal projections, an overlap of circumferential projections and no overlap of projection in any direction. The specific distribution of diagonally aligned defects is shown in Fig. 4(c). There is an overlap in the longitudinal projections between defects when  $S_L < 0$  and  $S_C > 0$ . There is an overlap in the circumferential projections between defects when  $S_L > 0$  and  $S_C < 0$ . There is no overlap of projection in any direction between defects when  $S_L > 0$  and  $S_C > 0$ .

The parameters influencing the diagonally aligned defects include the length and depth of defects and longitudinal and circumferential spacing. The geometries and spacings of diagonally aligned defects with and without overlap of projections are summarized in Table 8 and Table 9.

A pipeline containing a diagonal arrangement of defects with an overlap of longitudinal projections with  $L/\sqrt{Dt}=2.1$  and d/t=0.7 was used as a case. The effect of the variation in the overlapped distance of longitudinal projections on the failure process of the pipeline was analyzed. The distribution of von Mises stress from a negative to positive longitudinal spacing when  $S_C=0.01\pi D$  is given in Fig. 17. There is an overlap of longitudinal projections in Fig. 17(a)–(d). Fig. 17(e)–(f) shows diagonal defects without overlapping projections.

In Fig. 17(a)–(d), the stress at the spacing increases from 369 MPa to 409 MPa when the longitudinal spacing varies from  $-1.64 \sqrt{Dt}$  to  $-0.23 \sqrt{Dt}$ . Therefore, for diagonally aligned defects with an overlap of longitudinal projections, the interaction between defects gradually enhanced with the decrease in the overlapped distance of longitudinal projections. It is founded that the von Mises stress in the defect spacing reaches a maximum when  $S_L$  increases to  $d_1+d_2$ . It indicates that the interaction between defects is the most intense when the overlapped distance of longitudinal projections is the sum of the depths.

It can be seen from Fig. 17 that the circumferential spacing



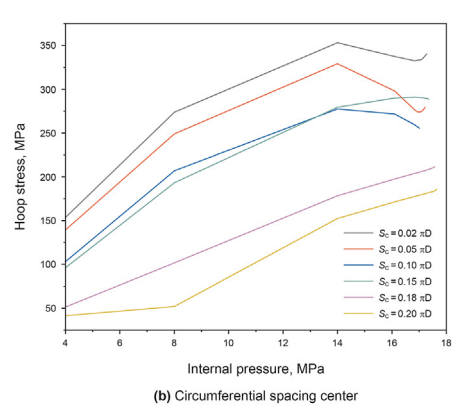


Fig. 14. The hoop stress at the center of the defect and spacing node for circumferentially aligned defects.

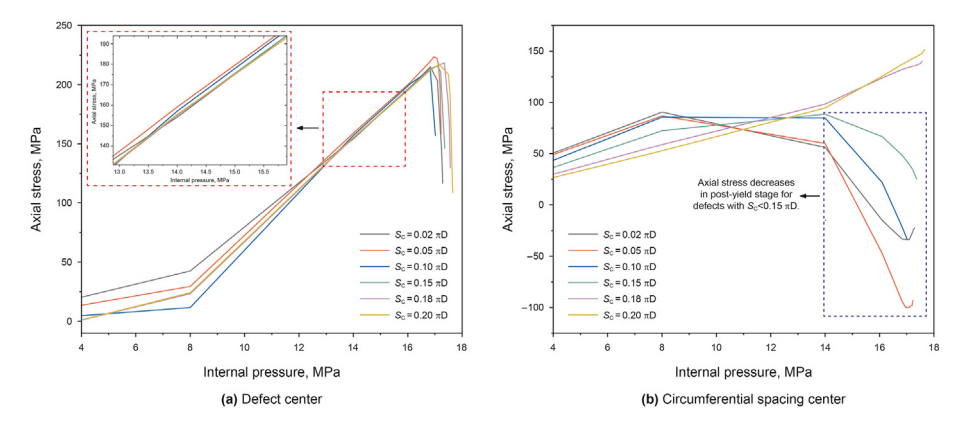


Fig. 15. The axial stress at the center of the defect and spacing node for circumferentially aligned defects.

**Table 7**Geometries and spacing of circumferentially aligned asymmetrical defects.

$L_1/\sqrt{Dt}$	$L_2/\sqrt{Dt}$	$d_1/t$	d <sub>2</sub> /t	$S_C/\pi D$
2.1	1.1, 1.6, 2.1	0.3, 0.5, 0.7	0.3, 0.4, 0.5, 0.6	0.02, 0.03, 0.05, 0.10, 0.15, 0.18, 0.20, 0.30
4.1	1.1, 2.1, 3.1, 4.1			
6.1	1.1, 2.1, 4.1, 6.1			

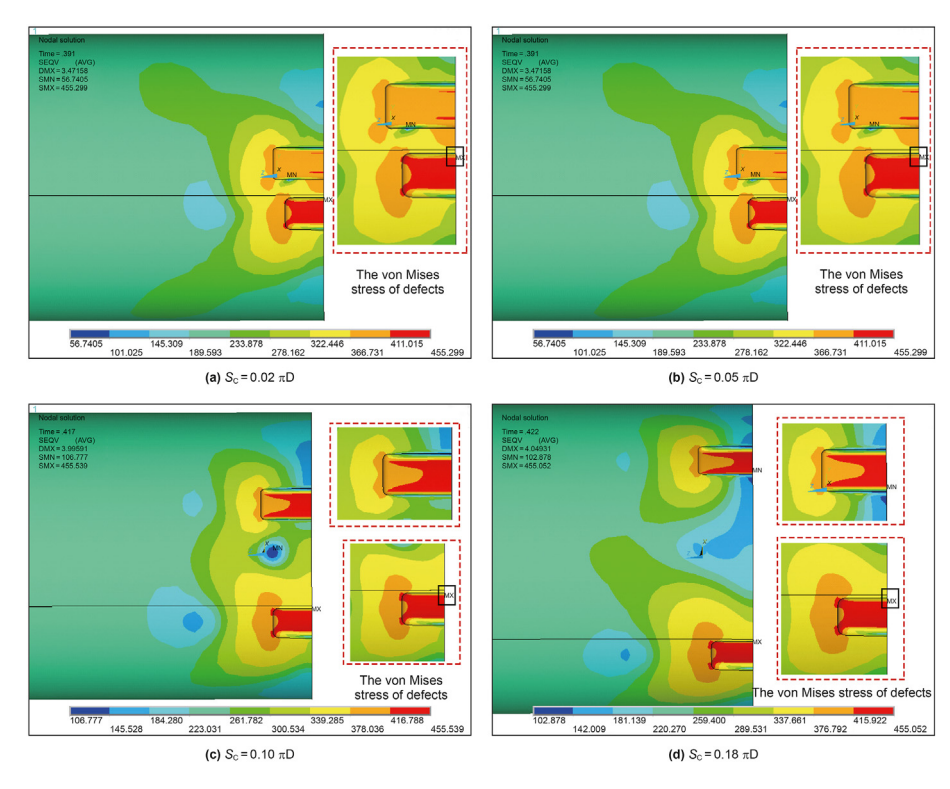


Fig. 16. The von Mises stress distribution of a pipeline containing circumferential asymmetrical defects with different circumferential spacing.

between defects results in a circumferential interaction. Moreover, it causes the failure position in the pipeline at the defect surface close to the circumferential spacing. Similarly, the failure position of the pipeline moves continuously with the increase of longitudinal spacing in the longitudinal direction. The pipeline failure generally occurs at the difference between the overlapped distance of longitudinal projections and the depth of the defect. In other words, the failure position appears at  $S_L + d_2$  of one side defect.

In Fig. 17(e)–(f), there is no overlap in the projections between

defects in any direction when  $S_L > 0$ . The burst failure position at the longitudinal boundary of one side of the defect, which is close to the longitudinal spacing. With an increase in longitudinal spacing, the von Mises stress at the line between defects and defect spacing and the interaction of defects decreases gradually. In summary, the increase in defect spacing will reduce the effect of interaction on the failure pressure of the pipeline containing diagonally aligned defects without an overlap of projections.

Fig. 18 depicts the distribution of von Mises stress at the burst

**Table 8**Geometries and spacings of diagonally aligned defects with an overlap of longitudinal projections and without overlap of projections.

$L/\sqrt{Dt}$	d/t	$S_L/\sqrt{Dt}$	$S_C/\pi D$
2.1	0.3	-1.41, -0.90, -0.40, -0.10, 0.40, 0.60, 0.90, 1.10, 1.60, 2.10	0.02, 0.05, 0.10, 0.15
	0.5	-1.62, -1.14, -0.65, -0.17, 0.47, 0.67, 0.97, 1.17, 1.67	0.02, 0.05, 0.10, 0.15
	0.7	-1.64, -1.71, -0.70, -0.23, 0.53, 0.73, 1.03, 1.23, 1.53, 1.73	0.01, 0.03, 0.05, 0.10, 0.15
4.1	0.3	-3.11, $-2.11$ , $-1.10$ , $-0.10$ , $0.40$ , $0.60$ , $0.90$ , $1.10$	0.02, 0.05, 0.10, 0.15
	0.5	-3.13, $-2.14$ , $-1.15$ , $-0.18$ , $0.47$ , $0.67$ , $0.97$ , $1.17$ , $1.67$	0.02, 0.05, 0.10, 0.15
	0.7	-3.15, -2.18, -1.21, -0.23, 0.53, 0.73, 1.03, 1.23, 1.73	0.01, 0.03, 0.05, 0.10, 0.15
6.1	0.3	-4.62, -3.11, -1.61, -0.10, 0.40, 0.60	0.02, 0.05, 0.10, 0.15
	0.5	-4.64, -3.15, -1.66, -1.067, -0.767, -0.17, 0.17, 0.47, 0.67, 1.17	0.02, 0.05, 0.10, 0.15
	0.7	-4.65, -3.18, -1.71, -0.23, 0.53, 0.73, 1.23, 1.73	0.01, 0.03, 0.05, 0.10, 0.15

**Table 9**Geometries and spacings of diagonally aligned defects with an overlap of circumferential projections and without overlap of projections.

L/ √Dt	d/t	$S_L/\sqrt{Dt}$	$S_C/\pi D$
2.1	0.3	0.40, 0.60, 0.90, 1.10, 1.60	-0.0281, -0.0205, -0.0129, -0.0053, 0.0253, 0.0353, 0.0453, 0.0553, 0.0853, 0.1053
	0.5	0.47, 0.67, 0.97, 1.17, 1.67	-0.0290, -0.0223, -0.0156, -0.0089, 0.0289, 0.0389, 0.0489, 0.0589, 0.0889, 0.1089
	0.7	0.53, 0.73, 1.03, 1.23, 1.73	-0.0299, -0.0241, -0.0183, -0.0125, 0.0225, 0.0325, 0.0425, 0.0525, 0.0625, 0.0925, 0.1125
4.1	0.3	0.40, 0.60, 0.90, 1.10	-0.0281, -0.0205, -0.0129, -0.0053, 0.0353, 0.0453, 0.0553, 0.1053
	0.5	0.47, 0.67, 0.97, 1.17	-0.0290, -0.0223, -0.0156, -0.0089, 0.0289, 0.0389, 0.0489, 0.0589, 0.0889, 0.1089, 0.1589
	0.7	0.53, 0.73, 1.03, 1.23	-0.0299, -0.0241, -0.0183, -0.0125, 0.0225, 0.0425, 0.0625, 0.0925, 0.1125
6.1	0.3	0.40, 0.60, 0.90	-0.0281, -0.0205, -0.0129, -0.0053, 0.0253, 0.0353, 0.0453, 0.0553, 0.0853, 0.1053
	0.5	0.47, 0.67, 0.97	-0.0290, -0.0223, -0.0156, -0.0089, 0.0289, 0.0389, 0.0489, 0.0589, 0.0889, 0.1089
	0.7	0.53, 0.73, 1.03	-0.0299, -0.0241, -0.0183, -0.0125, 0.0225, 0.0425, 0.0625, 0.0925, 0.1125, 0.1625

failure occurs for diagonally aligned defects with a length of  $L/\sqrt{Dt}=2.1$ , a depth of d/t=0.7, and a spacing of  $S_L/\sqrt{Dt}=0.3$ . It can be seen that the failure position barely appears to change. Therefore, the overlapping distance of circumferential projections has little effect on the burst failure position and the distribution of von Mises stress in the defect area. In general, the effect of the variation of the circumferential spacing on the interaction between defects is weak when the diagonally aligned defects have an overlap of circumferential projections.

For diagonally aligned defects with the overlap of circumferential projections in Fig. 18, the failure position in the longitudinal direction is observed to occur at the longitudinal boundary of the defect close to the longitudinal spacing. The position when the pipeline at burst failure occurs at the circumferential center of the defect. In addition, the burst failure position gradually shifts towards the region where  $S_C > 0$  because of the progressive strengthening of the circumferential interaction. Thus, it can be seen from Fig. 17(e) and (f) that the burst failure position transfers to the circumferential boundary of the defect when  $S_C > 0$ .

# 3.6. Comparison of interaction rules

According to the interaction rules summarized in Table 1, the applicability of different interaction rules was compared with the finite element results of adjacent defects simulated in this study. For adjacent defects of different arrangements, the identifications of the interaction rules are presented in Table 10. The percentages in Table 10 represent the proportion of cases in which the interacting defects identified by the rules are consistent with the FE results under one of the defect arrangements, which is calculated as follows:

$$p = \frac{n_i}{n_{Total}} \times 100\% \tag{1}$$

where  $n_i$  is the number of cases accurately identifying interacting defects by the criterion; i is one of the critical spacing rules; and  $n_{Total}$  is the number of FE examples in one defect arrangement.

According to Table 10, depending on the arrangement of defects, there are some differences in the accurate identification of interacting defects between different interaction rules. For longitudinally and circumferentially aligned defects, the interaction between asymmetrical defects is weaker than that between symmetrical defects by discussing the influence of the geometric consistency of adjacent defects on the stress state of the defect region. The stress state of the region of asymmetrical defects is mainly determined by whether the defect is longer or deeper. Therefore, the proposed interaction rules between defects are conservative for the identification of asymmetrical defects.

The interaction between circumferentially aligned defects is weaker than that between longitudinally aligned defects, so the circumferential limit spacing stipulated by most criteria is more restrictive. For example, the CW and POF rules ignore the interaction between defects when  $S_C = [0.05\pi D, 0.1\pi D]$ . Since the variation of increasing circumferential spacing on the interaction is not monotonic, the accuracy of identifications is poorer when  $S_C \leq 0.03\pi D$ . In addition, the circumferential limiting spacing proposed by Al-Owaisi et al. (2016) is too aggressive, and it ignores the factor of the increase in the interacting spacing corresponding to the shorter defect length. Therefore, the interaction between circumferentially aligned defects is often overlooked when using this criterion.

In diagonally aligned defects, the longitudinal and circumferential limit spacings are reduced when the defects have both longitudinal and circumferential interactions. Therefore, most of the rules are relatively conservative for interacting defects, which results in a lower predicted failure pressure than the actual failure pressure of the pipeline.

Fig. 19 depicts the average precision of identifications by the interaction rules for the interactions between adjacent defects. It can be seen that the interaction rule proposed by Li concerning different defect lengths has the highest identifications and can identify most of the interacting defects, followed by DNV RP-F101 and the worst CW rule.

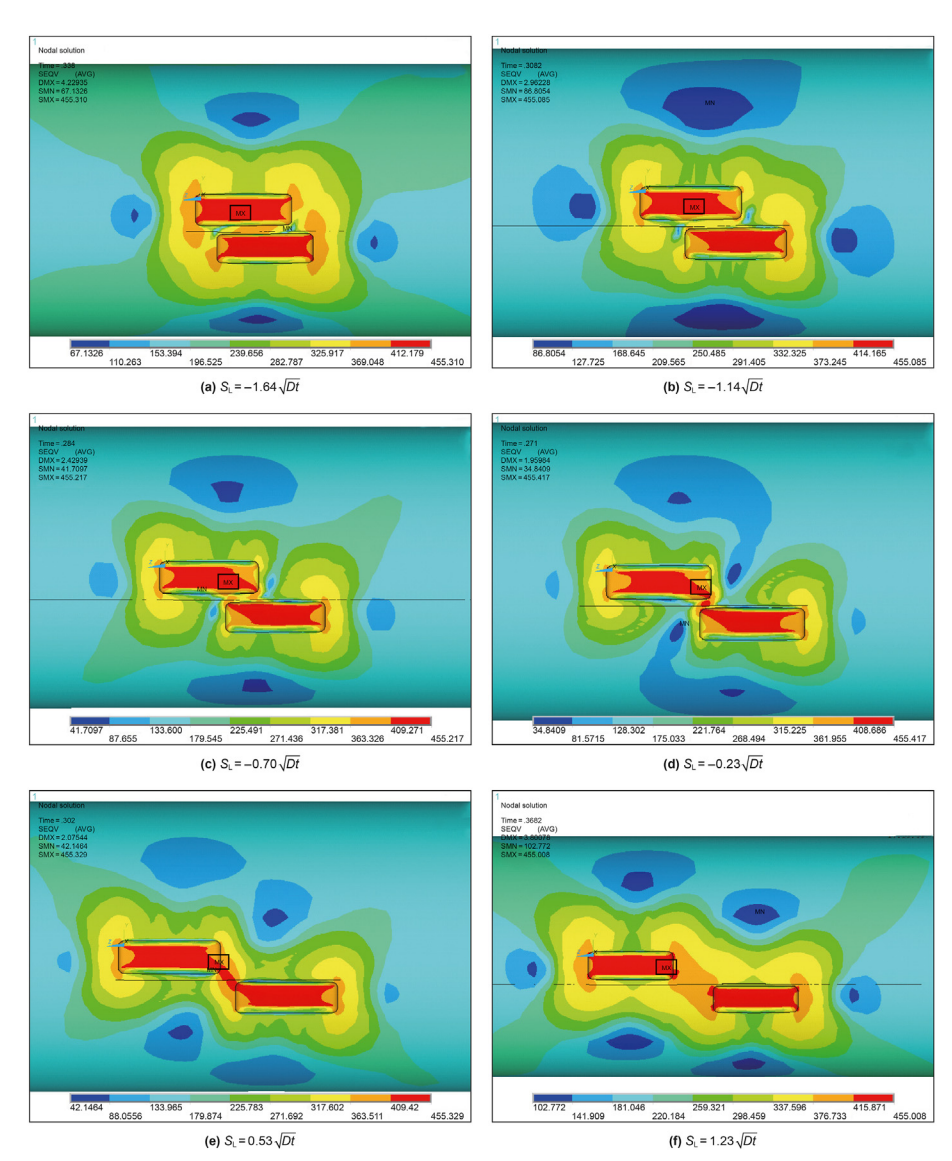


Fig. 17. The von Mises stress distribution of a pipeline containing diagonally aligned defects with different longitudinal spacings at circumferential spacing  $S_C = 0.01\pi D$ .

# 4. Conclusions

This study investigated the rule on the interaction between adjacent corrosion defects on a pipeline. The influence of the interaction between defects on the von Mises stress of a pipeline was analyzed, and the variation in the failure position with defect spacing under three arrangements was discussed. In addition, identifications by the interaction rules for adjacent defects of different arrangements were compared. The specific conclusions are as follows:

(1) For longitudinally aligned adjacent defects, regardless of whether their geometry is identical, the failure position of the pipeline is always located in the spacing area between the two defects connecting line when the longitudinal spacing is less than  $0.5 \sqrt{Dt}$ . With the increase of the defect spacing, the failure position of the pipeline containing symmetrical defects shifts from the center between the defect spacing to the center of one side defect; For asymmetrical defects, the failure position of the pipeline always moves

- from the spacing region to the defect center with relatively severe corrosion.
- (2) When the circumferential spacing is less than  $0.05\pi D$ , the failure position of the pipeline containing circumferentially symmetrically aligned defects occurs at the circumferential boundary of the defect far away from the defect spacing. As the defect spacing increases, the failure position of symmetrical defects first transfers to the circumferentially inner boundary of the defect near the spacing, and then gradually moves towards the defect center.
- (3) For overlapping defects diagonally aligned with projection in the axial direction, the interval from the spacing to the failure position of the pipe corresponds to the difference between the projected overlap distance and the depth of another defect (i.e., the distance from the defect spacing equals  $S_L + d_2$ ). For diagonally aligned defects with an overlap of circumferential projections, the influence of circumferential spacing variation on the failure position is negligible. For defects without projection overlap, the failure position appears at the defect endpoint close to the defect spacing on the path connecting the two defects.

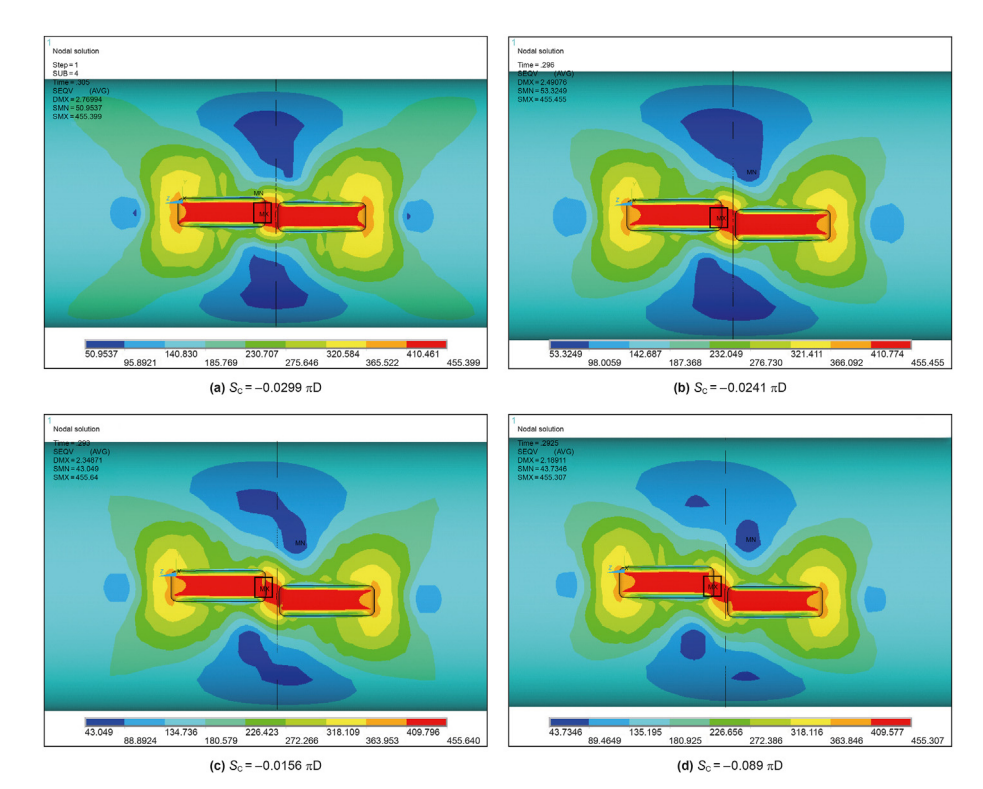


Fig. 18. The von Mises stress distribution of a pipeline containing diagonally aligned defects with different circumferential spacings at longitudinal spacing  $S_L = 0.3 \sqrt{Dt}$ .

**Table 10** Identifications of interactions between defects of different arrangements according to the interaction rules.

Cases	Numbers	CW	POF	DNV RP-F101	API 579	ASME B31G	BS 7910	Silva	Al-Owaisi	Li	Sun
Longitudinally aligned symmetrical defects	144	34.03%	70.83%	63.19%	77.08%	77.08%	63.19%	63.19%	77.08%	86.81%	51.39%
Longitudinally aligned asymmetrical defects	428	23.60%	63.32%	46.26%	77.57%	77.57%	46.26%	46.26%	77.57%	71.96%	29.44%
Circumferentially aligned symmetrical defects	214	54.67%	54.67%	76.64%	54.67%	51.40%	76.64%	70.56%	53.74%	71.03%	54.67%
Circumferentially aligned asymmetrical defects	342	71.93%	71.93%	71.05%	71.93%	67.54%	71.05%	77.19%	65.50%	78.07%	71.93%
Diagonally aligned defects	577	53.90%	57.89%	53.90%	62.39%	53.90%	53.90%	53.90%	57.89%	69.67%	53.90%

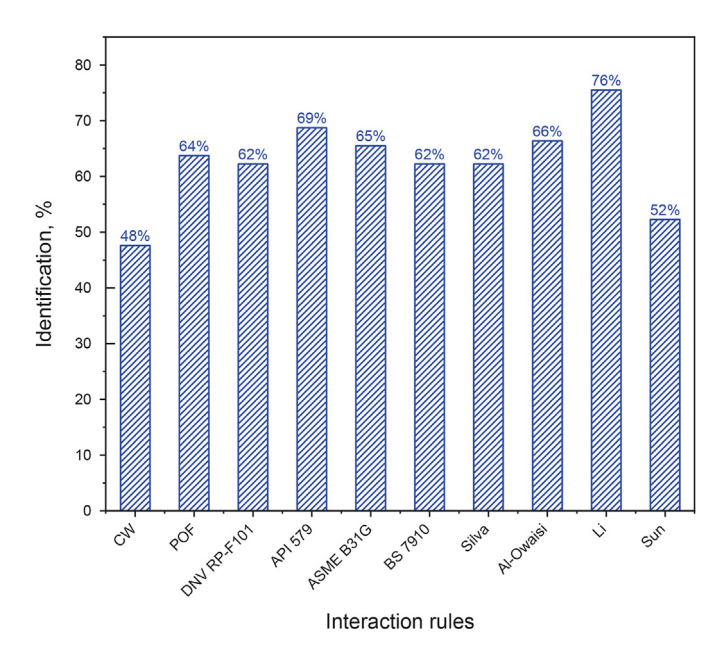


Fig. 19. Average identifications by the interaction rules.

(4) The current exist interaction rules are mostly developed or proposed based on the assumption of identical defect dimensions. Therefore, there are inevitably some application limitations. For asymmetrical defects, it is founded that these rules are relatively conservative to identify whether there is an interaction between defects. The identification result by these interaction rules is worst for diagonally aligned defects, followed by longitudinally aligned defects. When they are applied to circumferentially aligned defects, the identification effect is the most accurate. Among all these critical spacing rules, the one considering the defect length proposed by Li shows the highest accuracy in identifying the interacting defects.

It should be point out that some research conclusions of this work may be affected and limited by pipe specifications and pipe steel grades, such as high steel grade pipes, which need to be further studied in future work. However, the conclusions of this paper provide a reference for future research.

#### **Declaration of competing interest**

The authors declare that they have no known competing financial interests or personal relationships that could have appeared to influence the work reported in this paper.

#### Acknowledgements

This work was supported by the National Key R&D Program of China (Grant. No 2022YFC3004802-4), the Foundation of Sinopec (grant numbers 320034), the Strategic Cooperation Technology Projects of CNPC and CUPBZLZX2020-05, the Science Foundation of China University of Petroleum, Beijing (2462022YXZZ002), the Science Foundation of China University of Petroleum, Beijing (2462021YXZZ001).

#### References

- Al-Owaisi, S.S., Becker, A.A., Sun, W., 2016. Analysis of shape and location effects of closely spaced metal loss defects in pressurised pipes. Eng. Fail. Anal. 68, 172–186. https://doi.org/10.1016/j.engfailanal.2016.04.032.
- Al-Owaisi, S., Becker, A.A., Sun, W., Al-Shabibi, A., Al-Maharbi, M., Pervez, T., Al-Salmi, H., 2018. An experimental investigation of the effect of defect shape and orientation on the burst pressure of pressurised pipes. Eng. Fail. Anal. 93, 200–213. https://doi.org/10.1016/j.engfailanal.2018.06.011.
- American Petroleum Institute (API), 2007. Fitness-For-Service. API 579—1. Washington DC, USA.
- American Society of Mechanical Engineers, 2012. Manual for Determining the Remaining Strength of Corroded Pipelines: A Supplement to ASME B31 Code for Pressure Piping: an American National Standard. American Society of Mechanical Engineers.
- Bao, J., Zhou, W., 2021. Influence of depth thresholds and interaction rules on the burst capacity evaluation of naturally corroded pipelines. J. Pipeline Sci. Eng. 1, 148–165. https://doi.org/10.1016/j.jpse.2021.01.001.
- Benjamin, A.C., Cunha, D.J.S., 2007. New method for the prediction of the failure pressure of interacting corrosion defects. In: The Seventeenth International Offshore and Polar Engineering Conference. OnePetro.
- Benjamin, A.C., Freire, J.L.F., Vieira, R.D., Diniz, J.L., Andrade, E.Q., 2005. Burst tests on pipeline containing interacting corrosion defects. Int. Conf. Offshore Mech. Arctic Eng. 41979, 403–417. https://doi.org/10.1115/omae2005-67059.
- Benjamin, A.C., Freire, J.L.F., Vieira, R.D., 2007. Part 6: analysis of pipeline containing interacting corrosion defects. Exp. Tech. 31 (3), 74–82. https://doi.org/10.1111/j.1747-1567.2007.00190.x.
- Benjamin, A.C., Freire, J.L.F., Vieira, R.D., Cunha, D.J., 2016a. Interaction of corrosion defects in pipelines—Part 1: fundamentals. Int. J. Pres. Ves. Pip. 144, 56–62. https://doi.org/10.1016/j.ijpvp.2016.05.007.
- Benjamin, A.C., Freire, J.L.F., Vieira, R.D., Cunha, D.J., 2016b. Interaction of corrosion defects in pipelines—Part 2: MTI JIP database of corroded pipe tests. Int. J. Pres. Ves. Pip. 145, 41–59. https://doi.org/10.1016/j.ijpvp.2016.06.006.
- British Standard (BS), 2013. Guide to Methods for Assessing the Acceptability of Flaws in Metallic Structures, p. 7910. BS.
- Cabral, R.M., Ferreira, A.D., Pimentel, J.T., da Silva Cabral, M.A., Lyra, P.R., Afonso, S.M., Willmersdorf, R.B., 2022. Assessment by finite element modeling of pipelines with corrosion defects based on River-Bottom Profile model. Eng. Struct. 261, 114246. https://doi.org/10.1016/j.engstruct.2022.114246.
- Chauhan, V., Swankie, T., 2015. Guidance for Assessing the Remaining Strength of Corroded Pipelines (No. Report No. 9492).
- Chen, Y., Zhang, H., Zhang, J., Liu, X., Li, X., Zhou, J., 2015. Failure assessment of X80 pipeline with interacting corrosion defects. Eng. Fail. Anal. 47, 67–76. https://doi.org/10.1016/j.engfailanal.2014.09.013.
- Chen, Z.F., Chu, W.P., Wang, H.J., Li, Y., Wang, W., Meng, W.M., 2022. Structural integrity assessment of hydrogen-mixed natural gas pipelines based on a new multi-parameter failure criterion. Ocean Eng. 247. https://doi.org/10.1016/j.oceaneng.2022.110731.
- Cheng, F., 2016. Environmental hazard: monitor safety of aged fuel pipelines. Nature 529, 156. https://doi.org/10.1038/529156e.
- Chiodo, M.S.G., Ruggieri, C., 2009. Failure assessments of corroded pipelines with axial defects using stress-based criteria: numerical studies and verification analyses. Int. J. Pres. Ves. Pip. 86 (2–3), 164–176. https://doi.org/10.1016/j.ijpvp.2008.11.011.
- Cosham, A., Hopkins, P., 2004. An overview of the pipeline defect assessment manual (PDAM). In: 4th international pipeline technology conference, 29, pp. 720–745.
- Coulsen, K.E.W., Worthingham, R.G., 1990. New guidelines promise more accurate damage assessment. Oil Gas J. 88 (16).
- Cronin, D.S., Pick, R.J., 2002. Prediction of the failure pressure for complex corrosion defects. Int. J. Pres. Ves. Pip. 79 (4), 279–287. https://doi.org/10.1016/S0308-0161(02)00020-0.
- Det Norske Veritas (DNV), 2010. Corroded Pipelines—Recommended Practice: DNV

#### RP-F101: 2010. Norway.

- Fatemi, A., Kenny, S., 2011. Continuum modelling framework for local buckling response of plain and girth welded pipes. In: Offshore Technology Conference. OnePetro, https://doi.org/10.4043/21998-MS.
- Filho, J.E.A., Machado, R.D., Bertin, R.J., Valentini, M.D., 2014. On the failure pressure of pipelines containing wall reduction and isolated pit corrosion defects. Comput. Struct. 132, 22–33. https://doi.org/10.1016/j.compstruc.2013.10.017.
- Freire, J.L.F., Benjamin, A.C., Vieira, R.D., Diniz, J.L., 2011a. Strain analysis of pipeline test specimens containing longitudinal and circumferential corrosion defects. In: Applied Mechanics and Materials, vol. 70. Trans Tech Publications Ltd, pp. 422–427. https://doi.org/10.4028/www.scientific.net/AMM.70.422.
- Freire, J.L.F., Benjamin, A.C., Vieira, R.D., Diniz, J.L., 2011b. Burst strength of pipeline test specimens containing longitudinal or circumferential corrosion defects. In: Experimental and Applied Mechanics, ume 6. Springer, New York, NY, pp. 487–494. https://doi.org/10.1007/978-1-4614-0222-0\_59.
- Fu, J., Batte, A.D., 1999. An Overview of Advanced Methods for the Assessment of Corrosion in Linepipe.
- Gao, J., Yang, P., Li, X., Zhou, J., Liu, J., 2019. Analytical prediction of failure pressure for pipeline with long corrosion defect. Ocean Eng. 191, 106497. https://doi.org/ 10.1016/j.oceaneng.2019.106497.
- Idris, N.N., Mustaffa, Z., Seghier, M.E.A.B., Trung, N.T., 2021. Burst capacity and development of interaction rules for pipelines considering radial interacting corrosion defects. Eng. Fail. Anal. 121, 105124. https://doi.org/10.1016/ i.engfailanal.2020.105124.
- Kere, K.J., Huang, Q., 2022. Development of probabilistic failure pressure models for pipelines with single corrosion defect. Int. J. Pres. Ves. Pip. 197, 104656. https:// doi.org/10.1016/j.ijpvp.2022.104656.
- Keshtegar, B., Seghier, M.A.B., 2018. Modified response surface method basis harmony search to predict the burst pressure of corroded pipelines. Eng. Fail. Anal. 89, 177–199. https://doi.org/10.1016/j.engfailanal.2018.02.016.
- Li, X., Bai, Y., Su, C., Li, M., 2016. Effect of interaction between corrosion defects on failure pressure of thin wall steel pipeline. Int. J. Pres. Ves. Pip. 138, 8–18. https://doi.org/10.1016/j.ijpvp.2016.01.002.
- Liu, J., Chauhan, V., Ng, P., Wheat, S., Hughes, C., 2009. Remaining Strength of Corroded Pipe under Secondary (Biaxial) Loading (No. Report No. R9068). GL Industrial Services UK Ltd.
- Ma, B., Shuai, J., Liu, D., Xu, K., 2013. Assessment on failure pressure of high strength pipeline with corrosion defects. Eng. Fail. Anal. 32, 209–219. https://doi.org/10.1016/j.engfailanal.2013.03.015.
- McNealy, R., Gao, M., Limo'n-Tapia, S., Deaton, B., 2008. Defect assessment using effective area method from in-line inspection data. In: International Pipeline Conference, pp. 735–738. https://doi.org/10.1115/ipc2008-64481, 48586.
- Pitchford, J., 1999. Specification and requirements for the intelligent pig inspection of pipelines. Pipes Pipelines Int. 44 (1), 17–27, 1965.
- Shuai, Y., Wang, X.H., Li, J., Wang, J.Q., Wang, T.T., Han, J.Y., Cheng, Y.F., 2021. Assessment by finite element modelling of the mechano-electrochemical interaction at corrosion defect on elbows of oil/gas pipelines. Ocean Eng. 234, 109228. https://doi.org/10.1016/j.oceaneng.2021.109228.
- Shuai, Y., Zhang, X., Feng, C., Han, J., Cheng, Y.F., 2022a. A novel model for prediction of burst capacity of corroded pipelines subjected to combined loads of bending moment and axial compression. Int. J. Pres. Ves. Pip. 196, 104621. https://doi.org/10.1016/j.ijpvp.2022.104621.
- Shuai, Y., Zhang, X., Huang, H., Feng, C., Cheng, Y.F., 2022b. Development of an empirical model to predict the burst pressure of corroded elbows of pipelines by finite element modelling. Int. J. Pres. Ves. Pip. 195, 104602. https://doi.org/ 10.1016/j.ijpvp.2021.104602.
- Silva, R.C.C., Guerreiro, J.N.C., Loula, A.F.D., 2007. A study of pipe interacting corrosion defects using the FEM and neural networks. Adv. Eng. Software 38 (11–12), 868–875. https://doi.org/10.1016/j.advengsoft.2006.08.047.
- Soares, E., Bruère, V.M., Afonso, S.M.B., Willmersdorf, R.B., Lyra, P.R., Bouchonneau, N., 2019. Structural integrity analysis of pipelines with interacting corrosion defects by multiphysics modeling. Eng. Fail. Anal. 97, 91–102. https://doi.org/10.1016/j.engfailanal.2019.01.009.
- Sun, J.L., Cheng, Y.F., 2018. Assessment by finite element modeling of the interaction of multiple corrosion defects and the effect on failure pressure of corroded pipelines. Eng. Struct. 165, 278–286. https://doi.org/10.1016/j.engstruct.2018.03.040.
- Velázquez, J.C., González-Arévalo, N.E., Díaz-Cruz, M., Cervantes-Tobón, A., Herrera-Hernández, H., Hernández-Sánchez, E., 2022. Failure pressure estimation for an aged and corroded oil and gas pipeline: a finite element study. J. Nat. Gas Sci. Eng. 101, 104532. https://doi.org/10.1016/j.jngse.2022.104532.
- Wang, Y., Xu, L., Sun, J., Cheng, Y.F., 2021. Mechano-electrochemical interaction for pipeline corrosion: a review. J. Pipeline Sci. Eng. 1, 1–16. https://doi.org/10.1016/i.jpse.2021.01.002.
- Wang, Y., Xia, A., Zhang, P., Qin, G., 2022a. Probabilistic physical modeling of randomly corroded surface and its use in reliability analysis of corroded pipelines under spatiotemporal vibration. Ocean Eng. 262, 112219. https://doi.org/ 10.1016/j.oceaneng.2022.112219.
- Wang, Y., Xia, A., Qin, G., 2022b. Probabilistic modeling for reliability analysis of buried pipelines subjected to spatiotemporal earthquakes. Probabilist. Eng. Mech. 69, 103315. https://doi.org/10.1016/j.probengmech.2022.103315.
- Zhang, S., Zhou, W., 2020. Assessment of effects of idealized defect shape and width on the burst capacity of corroded pipelines. Thin-Walled Struct. 154, 106806. https://doi.org/10.1016/j.tws.2020.106806.
- Zhang, S., Zhou, W., 2021. Development of a burst capacity model for corroded

- pipelines considering corrosion defect width and a revised Folias factor equation. J. Nat. Gas Sci. Eng. 88, 103812. https://doi.org/10.1016/j.jngse.2021.103812. Zhang, S., Zhou, W., 2022. Assessment of the interaction of corrosion defects on steel pipelines under combined internal pressure and longitudinal compression using finite element analysis. Thin-Walled Struct. 171, 108771. https://doi.org/10.1016/j.tws.2021.108771.
- Zhou, R., Gu, X., Bi, S., Wang, J., 2022. Finite element analysis of the failure of highstrength steel pipelines containing group corrosion defects. Eng. Fail. Anal. 136, 106203. https://doi.org/10.1016/j.engfailanal.2022.106203.
- Zhu, X.K., 2021. A comparative study of burst failure models for assessing remaining strength of corroded pipelines. J. Pipeline Sci. Eng. 1 (1), 36–50. https://doi.org/10.1016/j.jpse.2021.01.008.